Article

Study on the Host-Guest Interactions Between Tetramethyl Cucurbit[6]uril and Benzimidazole Derivatives

YANG Naqin, DAI Xue, MA Yue, YANG Xinan and MA Peihua✉

Received March 24, 2023
Accepted April 26, 2023

In this paper, ^{1}H NMR spectroscopy, isothermal titration calorimetry, X-ray crystallography and other characterization methods were used to investigate the interaction modes of tetramethyl cucurbit[6]uril (TMeQ[6]) and three benzimidazole derivatives in an aqueous solution-solid state. The results showed that the aromatic ring moieties in the three derivatives all entered the cavity of TMeQ[6] and their substituents were located at the port of TMeQ[6], forming 1:1 host-guest inclusion complexes. The crystal structures showed that the aromatic part of the benzimidazole derivatives interacted with the cavity of TMeQ[6] *via* hydrogen bond interactions and the N atoms on the benzimidazole ring formed hydrogen bonds with the carbonyl oxygen of TMeQ[6]. The ion-dipole interactions between $[ZnCl_4]^{2-}$ and TMeQ[6] formed supramolecular self-assembly entities.

Keywords Tetramethyl cucurbit[6]uril (TMeQ[6]); Benzimidazole derivative; Host-guest interaction; Crystal structure

1 Introduction

Cucurbit[*n*]urils (Q[*n*]s)[1−5] have a rigid neutral electrostatic hydrophobic cavity, two negative electrostatic portal carbonyls, and a positive electrostatic outer surface. Their structural properties can be used to construct supramolecular framework materials with organic guest molecules, metal ions, and solitary pair electron neutral molecules or anions[6−10]. They can be used for the enrichment, separation, and recovery of metal ions[11,12], separation of isomers[13], the adsorption of volatile organic solvents[14,15], and supramolecular catalysis as a nanoreactor[16,17]. However, the rigid structure of conventional Q[*n*]s is not easily modified, so a series of modified Q[*n*]s have been reported. Tetramethyl cucurbit[6]uril (TMeQ[6]) is a derivative of Q[6][18], which leads to an increase in molecular polarity due to the introduction of methyl groups and exhibits high solubility in water. Compared with the spherical cavity of Q[*n*]s, TMeQ[6] has an elliptical cavity, which makes it exhibit higher selectivity for specific guest molecules[19]. The host-guest interactions formed between TMeQ[6] and aniline[20], halogenated hydrocarbons[21], pyridine[22,23], and bioamine[24], as well as the detection of La^{3+} or Ce^{3+} ions[25] have been reported.

Benzimidazole derivatives exhibit good biological activity and low toxicity, and the hydrogen atoms at the N-1 position are prone to tautomerization leading to their isomerization[26], which enables extensive structural modification[27]. Studies have shown that these derivatives have good antibacterial[28,29], antiviral[30], and anticancer[31] effects. Currently, interactions between benzimidazole derivatives and cucurbit[*n*=6—8]urils[32−35] and cyclohexanocucurbit[6]uril[36] have also been reported, while the studies on TMeQ[6] and benzimidazole derivatives have been less reported. In this paper, 2-aminobenzimidazole (G1), 2-hydroxymethylbenzimidazole (G2), 2-methylbenzimidazole (G3), and TMeQ[6] were selected as the objects to investigate the mode of interaction in an aqueous solution-solid state (Scheme 1). Consequently, the theoretical basis for studying the drug solubility, thermal stability, slow release, and biological activity has been provided through the construction of the Q[*n*]-benzimidazole derivative system.

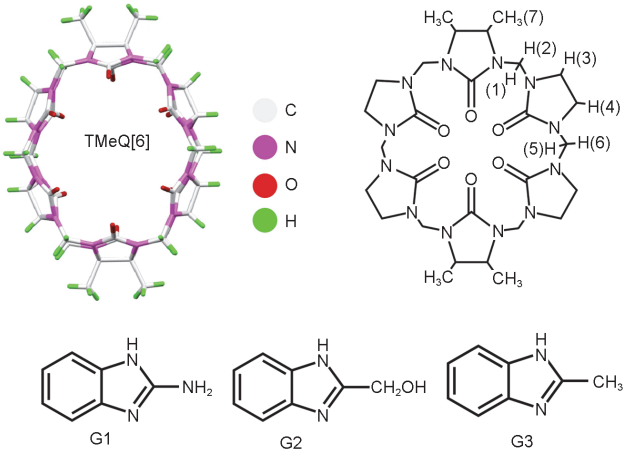

Scheme 1 Structural formula of TMeQ[6] in top view (up), 2-aminobenzimidazole (G1), 2-hydroxymethylbenzimidazole (G2), and 2-methylbenzimidazole (G3)

2 Experimental

2.1 General Materials

All materials were of reagent grade and used without any further purification. TMeQ[6] was prepared and purified in

✉ MA Peihua
phma@gzu.edu.cn
Key Laboratory of Macrocyclic and Supramolecular Chemistry of Guizhou Province, College of Chemistry and Chemical Engineering, Guizhou University, Guiyang 550025, P. R. China

https://doi.org/10.1007/s40242-023-3078-1

accordance to a literature method[18].

2.2 Complex Preparation

Complex **1**: TMeQ[6] (15 mg, 14.25 μmol) was dissolved in the hydrochloric acid solution (5 mL, 3 mol/L). $ZnCl_2$ (5.0 mg, 36.68 μmol) and 2-aminobenzimidazole (G1) (5.0 mg, 37.55 μmol) were then added to the resulting mixture and heated under reflux for >5 min. After cooling, the reaction mixture was filtered and the resulting solution was allowed to stand at room temperature for *ca*. 10 d. Crystals of $C_{47}H_{55}Cl_8N_{27}O_{13}Zn_2$ (complex **1**) suitable for single-crystal X-ray diffraction were formed. The yield was 36.8%.

Similarly, complexes **2** and **3** were prepared in the same way with yields of 45.01 and 37.21%, respectively.

2.3 Characterization

G1, G2, and G3 were prepared as aqueous solutions with concentrations of 1.0×10^{-3} mol/L, and TMeQ[6] was prepared as an aqueous solution with concentrations of 1.0×10^{-3} and 1.0×10^{-4} mol/L, respectively. The UV absorption spectra for the resulting solutions were obtained using the molar ratio method and equimolar continuous change method (Job's method), respectively[37].

G1, G2, and G3 with TMeQ[6] were prepared into 1.0×10^{-4} mol/L aqueous solutions of the inclusion complexes, which were allowed to stand for 30 min and then filtered twice using a 0.2 μm filter membrane. High-performance liquid chromatography-quadrupole time-of-flight mass spectrometry (HPLC-QTOF-MS) of the inclusion complexes was recorded on an Agilent 6545B instrument at room temperature.

All ^{1}H NMR spectroscopy data were recorded on a JEOL JNM-ECZ400s spectrometer in D_2O (pD=2.0) at 20 °C[20].

Isothermal titration calorimetry (ITC): the determination and data processing method was carried out using a procedure in the literature[38].

The thermal degradation of G1, G2, G3, and TMeQ[6], and their respective inclusion complexes was investigated using a BXT-TBDY-1250 thermoanalyzer instrument[39] under the N_2 atmosphere.

The X-ray crystal diffraction method used has been previously described in the literature[40]. The main crystal structure parameters are shown in Table S1 (see the Electronic Supplementary Material of this paper). In addition, the crystallographic data obtained for the reported structures have been deposited at the Cambridge Crystallographic Data Centre as supplementary publication [CCDC-2202501 (**1**), CCDC-2202502 (**2**), CCDC-2224645 (**3**)]. These data can be obtained free of charge *via* http://www.ccdc.cam.ac.uk/data request/cif.

3 Results and Discussion

3.1 UV-Vis Spectroscopy Analysis

UV-Vis absorption analysis was used to explore the interaction of G1, G2 and G3 with TMeQ[6] in the aqueous solution. Fig.1(A) shows the change in the UV-Vis absorption spectra of G1 with an increase in *n*(TMeQ[6]) and the inset exhibits the relationship between the absorption of G1 at the maximum absorption wavelength of 277 nm and *n*(TMeQ[6])/*n*(G1). It can be seen that increasing *n*(TMeQ[6]) gradually decreases the absorption of G1. When *n*(TMeQ[6])/*n*(G1)=1.0, the absorbance shows an obvious turning point. After increasing TMeQ[6], the change in the system absorption tends to become constant. The results show that G1 and TMeQ[6] form an inclusion complex with a 1:1 host-guest ratio. Fig.1(B) shows the experimental results obtained using the UV-Vis Job's method, which further confirmed that TMeQ[6] was bound to G1 and the mode of action was a molar ratio of 1:1. The UV-Vis absorption spectra obtained for TMeQ[6]-G2 and TMeQ[6]-G3 show the same phenomenon as TMeQ[6]-G1, in which G2 and G3 interact with TMeQ[6] with a host-guest binding ratio of 1:1 (Figs.S1 and S2, see the Electronic Supplementary Material of this paper).

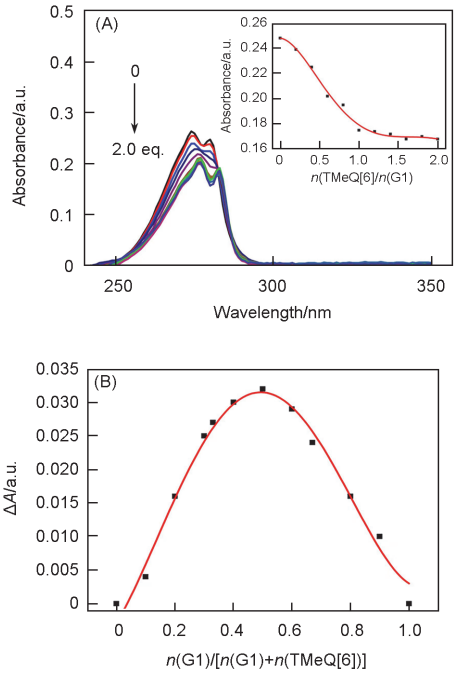

Fig.1 UV-Vis spectral changes of G1 (3.0×10^{-5} mol/L) upon stepwise addition of 0—2.0 molar equivalent TMeQ[6] in the aqueous solution (A) [inset: the corresponding absorbance changes at 277 nm *vs*. *n*(TMeQ[6])/*n*(G1)], and Jobs plot for TMeQ[6] and G1 in water by recording the absorbance changes at 277 nm (B)

3.2 HPLC-QTOF Mass Spectrometry Analysis

The HPLC-QTOF mass spectroscopic result provides further

https://doi.org/10.1007/s40242-023-3078-1

evidences for the inclusion complexes of G1, G2 and G3 with TMeQ[6], respectively. Obvious molecular peaks were observed at *m*/*z* 1186.4284, 1201.4273, and 1185.4331 (Fig.S3, see the Electronic Supplementary Material of this paper), which corresponded to G1@TMeQ[6] (1186.1020), G2@TMeQ[6] (1201.1130), and G3@TMeQ[6] (1185.1140), respectively. These molecular peaks further indicate that TMeQ[6] and G1—G3 form 1:1 host-guest inclusion complexes.

3.3 ^{1}H NMR Titration Spectroscopy Analysis

Simultaneously, we studied the host-guest interactions between TMeQ[6] and G1, G2, G3 *via* ^{1}H NMR titration spectroscopy method. Fig.2 shows ^{1}H NMR titration spectra obtained when different amounts of the G1 guest were added to the TMeQ[6] host. In the presence of *n*(G1)/*n*(TMeQ[6])= 1.00, the resonances for the aromatic protons (*α*-H, *β*-H) shifted upfield by *δ* 0.84 and 0.76, respectively, indicating that the G1 guest was encapsulated and an inclusion complex was formed. When further G1 was added, the free proton peak of G1 was observed, indicating that the TMeQ[6] host and G1 form a 1:1 host-guest inclusion. However, the position of the amino group in TMeQ[6] could not be determined using ^{1}H NMR spectroscopy. Fig.2 spectrum *d* shows that the proton peak of TMeQ[6] was shifted significantly, the resonances of H3, H4, H5 and H6 protons were shifted upfield by about *δ* 0.16, 0.39, 0.24 and 0.40, respectively. In contrast, the resonances of H1, H2 and H7 protons experienced downfield shifts of about *δ* 0.12, 0.05 and 0.07, respectively. We attributed this phenomenon to the shielding and deshielding effects of the aromatic ring in the guest molecule. When asymmetric guest molecules are encapsulated in the main cavity of TMeQ[6], it is impossible for the guest molecules to surround the axis of the elliptical cavity. As a result, the aromatic rings induce two different magnetic fields. Protons H3, H4, H5, and H6 were located in the shielded region, while protons H1, H2, and H7 were located in the deshielded region. At the same time, bimodal splitting of the main proton of TMeQ[6] was also observed, reflecting the two guest molecules approaching the two ports of TMeQ[6] from different ends.

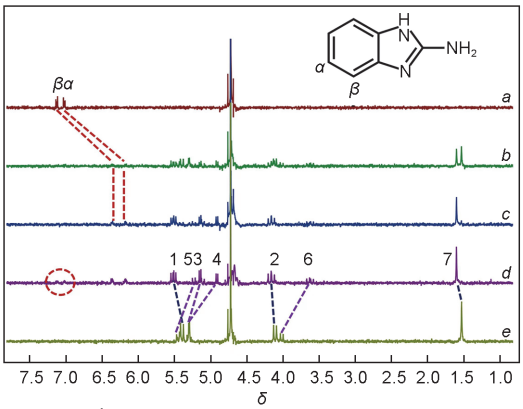

Fig.2 Titration ^{1}H NMR spectra (400 MHz, pD=2.0) of TMeQ[6] (5.0×10^{-4} mol/L) recorded by adding different molar equivalents of G1 at 20 °C

a. Neat G1; *b*. *n*(G1)/*n*(TMeQ[6])=0.50; *c*. *n*(G1)/*n*(TMeQ[6])=1.00; *d*. *n*(G1)/*n*(TMeQ[6])=1.20; *e*. neat TMeQ[6].

In the presence of *n*(G2)/*n*(TMeQ[6])=1.00, the resonance peaks observed for the aromatic protons (*α*-H, *β*-H) were shifted upfield by *δ* 0.74 and 0.82, respectively, and proton (*γ*-H) was shifted downfield by *δ* 0.01. These results show that the aromatic ring of G2 entered the cavity of TMeQ[6] and was shielded. The hydroxymethyl group was located at the port of TMeQ[6] and was deshielded, forming an inclusion complex with a 1:1 host-guest ratio (Fig.S4, see the Electronic Supplementary Material of this paper). In the presence of *n*(G3)/*n*(TMeQ[6])=1.00, the *α*-H and *β*-H protons experienced upfield shifts of *δ* 0.79 and 0.78, respectively. In contrast, the *γ*-H proton experienced a downfield shift of *δ* 0.01. These results show that the aromatic ring of G3 entered the cavity of TMeQ[6] and the methyl group was located at the port of TMeQ[6], forming an inclusion complex with a 1:1 host-guest ratio (Fig.S5, see the Electronic Supplementary Material of this paper). The chemical shift phenomenon of the proton peak of TMeQ[6] is the same as that in Fig.2 spectrum *d*, which is not described anymore.

3.4 Isothermal Titration Calorimetry Analysis

To better understand the host-guest interactions between TMeQ[6] and G1—G3, we carried out at least three ITC experiments to determine their thermodynamic parameters (Fig.S6, see the Electronic Supplementary Material of this paper). Table 1 shows the equilibrium association constants (K_a) and thermodynamic parameters for TMeQ[6]-benzimidazole derivatives interaction systems for G1, G2, and G3. The experimental results revealed K_a values ranging from 1.450×10^4 L/mol to 5.310×10^5 L/mol and negative ΔG values ranging from –28.02 kJ/mol to –32.68 kJ/mol for TMeQ[6]-G*n* interactions. Thus, these three benzimidazole derivatives could effectively bind to the TMeQ[6] host. Based on the Gibbs free energy ($\Delta G=-RT\ln K_a=\Delta H-T\Delta S$), it can be inferred that all three reactions are exothermic and appear to be driven by favorable enthalpy changes.

Table 1 Thermodynamic parameters of the interactions formed between TMeQ[6] and the guest molecules (G1—G3)

Complex	K_a/(L·mol^{-1})	ΔH/(kJ·mol^{-1})	$T\Delta S$/(kJ·mol^{-1})	ΔG/(kJ·mol^{-1})
TMeQ[6]-G1	8.098×10^4	–29.17	–1.15	–28.02
TMeQ[6]-G2	5.310×10^5	–100.00	–67.32	–32.68
TMeQ[6]-G3	1.450×10^4	–68.90	–39.44	–29.46

3.5 Thermogravimetric Analysis

Thermogravimetric analysis (TGA) and differential

https://doi.org/10.1007/s40242-023-3078-1

thermogravimetry (DTG) of G1, G1@TMeQ[6], and TMeQ[6] are shown in Fig.3. Fig.3(A) shows that G1 has good thermal stability at 50—260 °C and starts to lose mass from 260 °C. The quality was reduced by 67.38%. In the other two curves, there was one mass degradation region between 50 and 240 °C. The mass loss was due to the loss of water (crystallizing water) and the mass was reduced by 14.47%. TMeQ[6] began to decompose at 370 °C with a mass loss of 50.51%, while the inclusion complex of G1@TMeQ[6] was decomposed at 340 °C with a mass loss of 53.07%. These results indicate that the G1@TMeQ[6] inclusion complex has a higher decomposition temperature, less mass variation, and better thermal stability than G1 alone. G1 has two endothermic peaks at 322.0 and 408.2 °C. TMeQ[6] has a sharp melting heat absorption peak at 417.9 °C. For the G1@TMeQ[6] complex, the melting absorption peaks of G1 at 322.0 °C and TMeQ[6] at 417.9 °C disappear, while new endothermic decomposition peaks appear at 410.9 °C [Fig.3(B)]. This indicates that G1 and TMeQ[6] were involved in the host-guest inclusion complex and the endothermic decomposition peak of the inclusion complex shifted towards the high temperature, indicating that the formed inclusion complex was more stable than G1.

G2 resolved at 220 °C with a mass reduction of 62.19% and the G2@TMeQ[6] inclusion complex was resolved at 271 °C with a mass loss of 58.91%. G2 shows one endothermic double peak at 290.5 and 336.0 °C and one endothermic peak at 533.0 °C. For the G2@TMeQ[6] complex, the melting point endothermal peak of G2 at 336 °C disappeared, while a new endothermic decomposition peak appeared at 501.0 °C (Fig.S7, see the Electronic Supplementary Material of this paper). The decomposition of G3 occurred at 183 °C and was completely decomposed at 285 °C with a mass reduction of 99.68%. G3@TMeQ[6] was resolved at 375 °C with a mass loss of 52.89%. There was a sharp thermal absorption peak at 268 °C in G3. For the G3@TMeQ[6] complex, the melting heat absorption peak of G2 at 268 °C disappeared, while a new thermal decomposition peak appeared at 405 °C (Fig.S8, see the Electronic Supplementary Material of this paper). This indicates that G2 and G3 interact with TMeQ[6]. The shift in the endothermic decomposition peak of the inclusion complex towards the high temperature indicates that the inclusion complex has a better thermal stability than G2 and G3 alone.

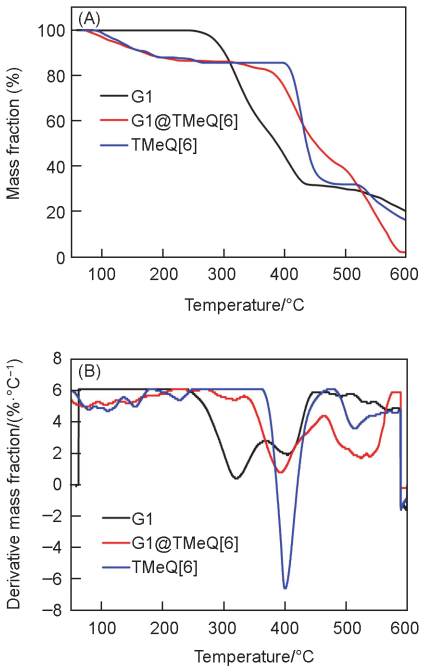

Fig.3 TGA (A) and DTG (B) curves of G1, G1@TMeQ[6], and TMeQ[6]

3.6 Description of Crystal Structures

In the presence of structure-directing agent $[ZnCl_4]^{2-}$ anions, we obtained single crystals of the complexes **1**—**3** by slow vapor evaporation. Complex **1** exhibits a triclinic $P\bar{1}$ space group. Fig.4 shows that TMeQ[6] and G1 form a 1:1 host-guest inclusion complex. In this system, hydrogen bonding is one of the main interactions. N13 forms three hydrogen bonds with O1, O5, and O6, and N15 forms three hydrogen bonds with O2, O3, and O4; the N—H···O hydrogen bond lengths were in the range of 2.597—3.047 Å (1 Å=0.1 nm) [Fig.4(A)]. In addition, the amino groups also form hydrogen bond interactions with TMeQ[6] connected *via* N14—O9 with a distance of 2.772 Å [Fig.4(B)]. The port carbonyl oxygen of TMeQ[6] forms self-induced dipole interactions with the methine units and bridged methylene units of another TMeQ[6] and the interaction distance was 2.649 Å (blue curves). TMeQ[6] forms a hydrogen bond with a free water molecule (O2—O13) and the interaction distance was 2.177 Å. Fig.4(C) shows the aromatic ring in G1 enters the cavity of TMeQ[6] forming hydrogen bond interactions with the port carbonyl group on TMeQ[6] *via* C—H48···C30 and C—H48···C44 (black curves). Ion-dipole interactions (C—H···Cl interactions) were formed between the structural inducer $[ZnCl_4]^{2-}$ anion and the methine units and bridged methylene units of TMeQ[6] [Fig.4(D)]. Fig.5 shows the structural stacking diagram of the complex viewed along the *b*-axis and *c*-axis. $[ZnCl_4]^{2-}$ anions surround TMeQ[6] molecules and connect TMeQ[6] molecules to form supramolecular self-assembly entities *via* ion-dipole interactions. Complex **1** has an obvious pore and a layered framework structure with a pore area of *ca.* 136 Å^2.

Complex **2** exhibits a monoclinic *C*2/*c* space group. The aromatic ring in G2 was located in the cavity of TMeQ[6] and the N atoms on the imidazole ring form hydrogen bond interactions with the carbonyl oxygen on TMeQ[6], namely N1—O1, N1—O2, N2—O4, and N2—O6, and their distances are 2.814 , 2.758 , 2.927, and 2.917 Å, respectively. The cavity of TMeQ[6] forms hydrogen bond interactions with the aromatic

https://doi.org/10.1007/s40242-023-3078-1

ring (C—H27···O6, C—H20···N11) with distances of 2.719 and 2.711 Å, respectively. The $[ZnCl_4]^{2-}$ anions connect the four TMeQ[6] molecules *via* C—H···Cl interactions and form a supramolecular self-assembly (Fig.6). Complex **3** exhibits a monoclinic *Cc* space group. The N atoms on the benzimidazole ring in G3 form hydrogen bonds with the carbonyl oxygen on TMeQ[6], which are N25—O1, N25—O2, N26—O4, and N26—O5, and their interaction distances are 2.740, 2.685, 2.879, and 2.728 Å, respectively. The aromatic ring in G3 forms hydrogen bond interactions with the N atom of TMeQ[6] (C—H44···N5, C—H44···N6) with distances of 2.742 and 2.728 Å, respectively. The free water molecules form hydrogen bonds with the carbonyl group of TMeQ[6] (O1W—O11 and O1W—O12) and the guest molecules (C—H42···O1W) with distances of 1.978 , 1.931, and 2.610 Å, respectively. The free water molecules act as bridges to form a one-dimensional supramolecular chain (Fig.7).

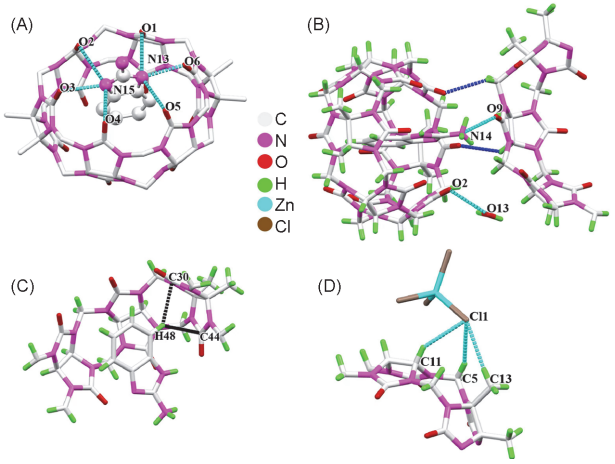

Fig.4 Hydrogen bond interactions between G1 molecule and portal carbonyls (A) or the cavity (C) of TMeQ[6], hydrogen bond and dipole interactions (B), and ion dipole interactions (D) of complex 1

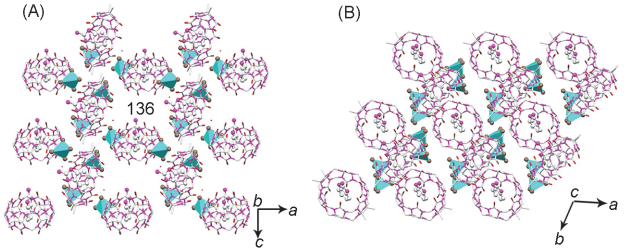

Fig.5 Structural stacking diagrams of complex 1 viewed along *b* (A) and *c* axis (B)

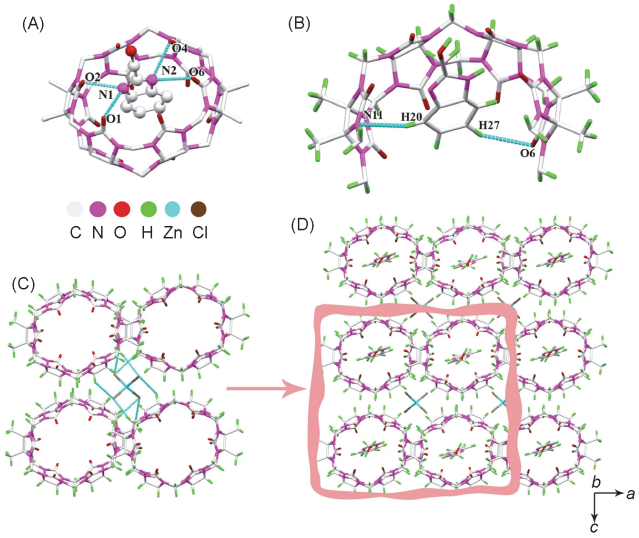

Fig.6 Hydrogen bond interactions between G2 molecule and portal carbonyls (A) or the cavity (B) of TMeQ[6], ion dipole interactions (C), and structural stacking diagram (D) of complex 2 viewed along the *b*-axis

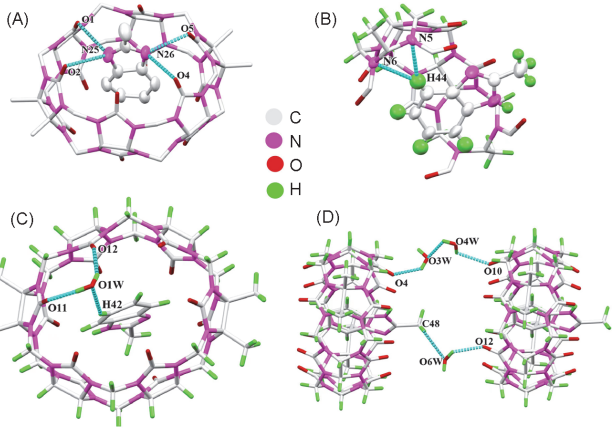

Fig.7 Hydrogen bond interactions between G3 molecule and portal carbonyls (A) or the cavity (B) of TMeQ[6], hydrogen bond interactions of free water molecules with the guest G3 and TMeQ[6] (C), and one-dimensional supramolecular chain (D)

4 Conclusions

In summary, we have investigated the host-guest complexation of TMeQ[6] with three benzimidazole derivatives by UV-Vis spectroscopy, HPLC-QTOF mass spectrometry, ^{1}H NMR spectroscopy, ITC, thermoanalysis instrument, and X-ray crystallography techniques. The results show that the aromatic rings of three benzimidazole derivatives enter the cavity of TMeQ[6] and their substituents are located at the port of TMeQ[6], forming 1:1 host-guest complexes. The shift in the endothermic decomposition peak of the inclusion complex towards the high temperature indicates that the inclusion complex has better thermal stability than G1, G2, and G3 alone. The crystal structures show that the aromatic part of the benzimidazole derivatives interact with the cavity of TMeQ[6] *via* hydrogen bond interactions and the N atoms on the benzimidazole ring form hydrogen bonds with the carbonyl oxygen of TMeQ[6]. The ion-dipole interactions of $[ZnCl_4]^{2-}$ cause the adjacent TMeQ[6] molecules to stack and form a supramolecular self-assembly. Consequently, the theoretical basis for studying the drug solubility, thermal stability, slow release, and biological activity has been provided through the construction of the

https://doi.org/10.1007/s40242-023-3078-1

Q[*n*]-benzimidazole derivative system.

Electronic Supplementary Material

Supplementary material is available in the online version of this article at http://dx.doi.org/10.1007/s40242-023-3078-1.

Acknowledgements

This work was supported by the National Natural Science Foundation of China (No.22161010).

Conflicts of Interest

The authors declare no conflicts of interest.

References

[1] Freeman W. A., Mock W. L., Shih N. Y., *J. Am. Chem. Soc.*, **1981**, *103*, 7367
[2] Kim J., Jung I. S., Kim S. Y., Lee E., Kang J. K., Sakamoto S., Yamaguchi K., Kim K., *J. Am. Chem. Soc.*, **2000**, *122*, 540
[3] Liu S. M., Zavalij P. Y., Isaacs L., *J. Am. Chem. Soc.*, **2005**, *127*, 16798
[4] Li Q., Qiu S. C., Zhang J., Chen K., Huang Y., Xiao X., Zhang Y. J., Li F., Zhang Y. Q., Xue S. F., Zhu Q. J., Tao Z., Lindoy L. F., Wei G., *Org. Lett.*, **2016**, *18*, 4020
[5] Cheng X. J., Liang L. L., Chen K., Ji N. N., Xiao X., Zhang J. X., Zhang Y. Q., Xue S. F., Zhu Q. J., Ni X. L., Tao Z., *Angew. Chem. Int. Ed.*, **2013**, *52*, 7252
[6] Chen K., Hua Z. Y., Zhao J. L., Redshaw C., Tao Z., *Inorg. Chem. Front.*, **2022**, *9*, 2753
[7] Yang D., Liu M., Xiao X., Tao Z., Redshaw C., *Coordin. Chem. Rev.*, **2021**, *434*, 213733
[8] Chen K., Ge W. W., Xu J., Zhang S. M., Li Y. W., Hua Z. Y., Tao Z., *J. Mol. Struct.*, **2019**, *1181*, 220
[9] Shen F. F., Zhao J. L., Chen K., Hua Z. Y., Chen M. D., Zhang Y. Q., Zhu Q. J., Tao Z., *CrystEngComm*, **2017**, *19*, 2464
[10] Ni X. L., Xue S. F., Tao Z., Zhu Q. J., Lindoy L. F., Wei G., *Coordin. Chem. Rev.*, **2015**, *287*, 89
[11] Wu H., Wang Y., Jones L. O., Liu W. Q., Zhang L., Song B., Chen X. Y., Stern C. L., Schatz G. C., Stoddart J. F., *Angew. Chem. Int. Ed.*, **2021**, *60*, 17587
[12] Wu H., Jones L. O., Wang Y., Shen D. K., Liu Z. C., Zhang L., Cai K., Jiao Y., Stern C. L., Schatz G. C., Stoddart J. F., *ACS Appl. Mater. Interfaces*, **2020**, *12*, 38768
[13] Shan P. H., Tu S. C., Lin R. L., Tao Z., Liu J. X., Xiao X., *CrystEngComm*, **2017**, *19*, 2168
[14] Wang C. Z., Zhao W. X., Shen F. F., Zhang Y. Q., Zhu Q. J., Xiao X., Tao Z., *CrystEngComm*, **2016**, *18*, 2112
[15] Qu Y. X., Zhou K. Z., Chen K., Zhang Y. Q., Xiao X., Zhou Q. D., Tao Z., Ma P. H., Wei G., *Inorg. Chem.*, **2018**, *57*, 7412.
[16] Rad N., Sashuk V., *Chem. Commun.*, **2022**, *58*, 5249
[17] Tang B. H., Zhao J. T., Xu J. F., Zhang X., *Chem. Eur. J.*, **2020**, *26*, 15446
[18] Zhao Y. J., Xue S. F., Zhu Q. J., Tao Z., Zhang J. X., Wei Z. B., Long L. S., Hu M. L., Xiao H. P., Day A. I., *Chin. Sci. Bull.*, **2004**, *49*, 1111
[19] Lin R. L., Fang G. S., Sun W. Q., Liu J. X., *Scl. Rep.*, **2016**, *6*, 39057
[20] Meng Y., Zhao W. W., Zheng J., Jiang D. F., Gao J., Jin Y. M., Ma P. H., *RSC Adv.*, **2021**, *11*, 3470
[21] Xiao X., Gao Z. Z., Shan C. L., Tao Z., Zhu Q. J., Xue S. F., Liu J. X., *Phys. Chem. Chem. Phys.*, **2015**, *17*, 8618
[22] Cong H., Tao L. L., Yu Y. H., Tao Z., Yang F., Zhao Y. J., Xue S. F., Lawrance G. A., Wei G., *J. Phys. Chem. A*, **2007**, *111*, 2715
[23] Yang B., Xiao X., Zhang Y. Q., Zhu Q. J., Xue S. F., Tao Z., Wei G., *RSC Adv.*, **2014**, *4*, 44359
[24] Yang L. G., Kan J. L., Wang X., Zhang Y. H., Tao Z., Liu Q. Y., Wang F., Xiao X., *Front. Chem.*, **2018**, *6*, 289
[25] Huang Y. H., Geng Q. X., Jin X. Y., Cong H., Qiu F., Xu L., Tao Z., Wei G., *Sensor. Actuat. B*: *Chem.*, **2017**, *243*, 1102
[26] Akhtar W., Khan M. F., Verma G., Shaquiquzzaman M., Rizvi M. A., Mehdi S. H., Akhter M., Alam M. M., *Eur. J. Med. Chem.*, **2017**, *126*, 705
[27] Bistrović A., Krstulović L., Stolić I., Drenjančević D., Talapko J., Taylor M. C., Kelly J. M., Bajić M., Raić-Malić S., *J. Enzym. Inhib. Med. Chem.*, **2018**, *33*, 1323
[28] Arora R. K., Kaur N., Bansal Y., Bansal G., *Acta Pharm. Sin. B*, **2014**, *4*, 368
[29] de Oliveira H. C., Rodrigues M. L., *Fungal. Biol. Rev.*, **2021**, *37*, 27
[30] Tonelli M., Novelli F., Tasso B., Vazzana I., Sparatore A., Boido V., Sparatore F., la Colla P., Sanna G., Giliberti G., Busonera B., Farci P., Ibba C., Loddo R., *Bioorgan. Med. Chem.*, **2014**, *22*, 4893
[31] Wu L. T., Jiang Z., Shen J. J., Yi H., Zhan Y. C., Sha M. Q., Wang Z., Xue S. T., Li Z. R., *Eur. J. Med. Chem.*, **2016**, *114*, 328
[32] Ge J. Y., Xue S. F., Zhu Q. J., Tao Z., Zhang J. X., *J. Incl. Phenom. Macro.*, **2007**, *58*, 63
[33] Zhao Y. J., Pourgholami M. H., Morris D. L., Collins J. G., Day A. I., *Org. Biomol. Chem.*, **2010**, *8*, 3328
[34] Albdallah S. K., Assaf K. I., Bodoor K., Al-Sakhen N. A., Malhis L. D., Alhmaideen A. I., El-Barghouthi M. I., *J. Solution. Chem.*, **2018**, *47*, 1768
[35] Wang Q., Guo J. Z., Luo D., Ye M. F., Lin R. L., Sun W. Q., Liu J. X., *Phys. Chem. Chem. Phys.*, **2022**, *24*, 25930
[36] Zheng L. M., Zhang K., Lin R. L., Chu X. F., Liu J. X., *J. Incl. Phenom. Macro.*, **2020**, *96*, 125
[37] Lu Y., Yu Z. C., Yang X. N., Dai J. J., Shan P. H., Feng X. H., Tao Z., Redshaw C., Xiao X., *Chin. Chem. Lett.*, **2022**, 108040
[38] Qu Y. X., Lin R. L., Zhang Y. Q., Zhou K. Z., Zhou Q. D., Zhu Q. J., Tao Z., Ma P. H., Liu J. X., Wei G., *Org. Chem. Front.*, **2017**, *4*, 1799
[39] Shi Z. L., Liu X. K., Zhou Y. H., Cong H., *Polym. Adv. Technol.*, **2022**, *33*, 2498
[40] Zheng J., Ma Y., Yang X. N., Ma P. H., *RSC Adv.*, **2022**, *12*, 18736